https://doi.org/10.5194/hess-2020-590
Preprint. Discussion started: 21 November 2020

Hydrology and Earth System Sciences
Discussions

Long-term relative decline in evapotranspiration with increasing runoff on fractional land surfaces

Ren Wang[1, 2], Pierre Gentine[3, 4], Jiabo Yin[5], Lijuan Chen[1, 2], Jianyao Chen[6], Longhui Li[1, 2]

[1]School of Geographical Sciences, Nanjing Normal University, Nanjing 210023, China
[2]Key Laboratory for Geographical Environment Evolution, Ministry of Education, Nanjing, 210023, China
[3]Earth and Environmental Engineering Department, Columbia University, New York, NY 10027, USA
[4]Earth Institute, Columbia University, New York, NY 10025, USA
[5]State Key Laboratory of Water Resources and Hydropower Engineering Science, Wuhan University, Wuhan 430072, China
[6]School of Geography and Planning, Sun Yat-sen University, Guangzhou 510275, China

Correspondence to: Ren Wang (wangr67@mail2.sysu.edu.cn)

Abstract. Evapotranspiration (ET) accompanied by water and heat transport in the hydrological cycle is a key component in regulating surface aridity. Existing studies documenting changes in surface aridity have typically estimated ET using semi-empirical equations or parameterizations of land surface processes, which are based on the assumption that the parameters in the equation are stationary. However, plant physiological effects and its responses to a changing environment are dynamically modifying ET, thereby challenging this assumption and limiting the estimation of long-term ET. In this study, the latent heat flux (ET in energy units) and sensible heat flux were retrieved for recent decades on a global scale using machine learning approach and driven by ground observations from flux towers and weather stations. The study resulted in several findings, namely that the evaporative fraction (EF)—the ratio of latent heat flux to available surface energy—exhibited a relatively decreasing trend on fractional land surfaces; In particular, the decrease in EF was accompanied by an increase in long-term runoff as assessed by precipitation (P) minus ET, accounting for 27.06% of the global land areas. The signs were indicative of reduced surface conductance, which further emphasized that land-surface vegetation has major impacts in regulating the water and energy cycles, as well as aridity variability.

1 Introduction

Evapotranspiration (ET) mainly includes two processes: (1) evaporation from soil and plant surfaces and (2) transpiration from plants to the atmosphere. These processes connect the transfer of moisture and energy in soil, vegetation, and atmospheric systems (Miralles et al., 2020; Salvucci et al., 2013; Yang et al., 2020). Quantifying changes in the exchange of moisture and heat between the land and atmosphere is very important for understanding and characterizing water and energy cycles, which has implications in various fields such as hydrology, climatology, and agronomy (Hoek van Dijke et al., 2020; Gentine et al., 2016; Komatsu and Kume, 2020).

https://doi.org/10.5194/hess-2020-590
Preprint. Discussion started: 21 November 2020


Hydrology and Earth System Sciences
Discussions

ET is expected to intensify with the warming climate, thereby contributing to the increase in surface aridity stress (Baruga et al., 2020; Berg et al., 2016; Fu et al., 2014; Trenberth et al., 2014). However, quantification of changes in aridity/wetness was usually derived from traditional offline drought indices such as the Standardized Precipitation Evapotranspiration Index, which embedded a semi-empirical equation, e.g., the Penman–Monteith equation, for ET estimation (Dai et al., 2013; Sheffield et al., 2012). Using potential evaporation rather than actual ET or taking ET output from a climate model as the input of traditional offline drought indices, the calculation assumes that soil can always supply moisture to meet the atmospheric evaporative demand, which is an incorrect assumption for most land surfaces (Greve et al., 2014; Milly and Dunn, 2016; Yang et al., 2020). Moreover, when using a semi-empirical equation for ET estimation, some parameters such as soil resistance and stomatal resistance, are assumed to be stationary over time; however, we know that these parameters are continually changing with environmental conditions (Miralles et al., 2011; Yang et al., 2019; Zhou et al., 2016).

Why are the soil resistance and stomatal resistance not stationary? Changes in plant stomata and leaf area, with increasing CO_2 concentrations in particular, reshape the allocation of surface energy and affect transpiration (Forzieri et al., 2020; Sorokin et al., 2017; Mallick et al., 2016; Williams and Torn, 2015). With increasing CO_2 concentrations, the density and opening degree of leaf stomata decrease, while the water-use efficiency and biomass production of plant increase, thus modifying transpiration rate (Keenan et al., 2013; Massmann et al., 2019; Rigden et al., 2016; van Der Sleen et al., 2015; Wagle et al., 2015). Vegetation transpiration occupies most of the amount of ET, so vegetation controls can greatly affect the variability of land ET (Costa et al., 2010; Jaramillo et al., 2018; Wei et al., 2017; Williams et al., 2012). Moreover, human activities including agricultural irrigation and land use management, are constantly altering the exchange of water and heat between terrestrial ecosystems and the atmosphere (Padrón et al., 2020; Teuling et al., 2019). The semi-empirical equations of ET and offline drought indices also prove challenging when taking these effects into consideration (Yang et al., 2020). Existing studies with respect to global ET inferred from flux towers, remote sensing, and reanalysis products have a relatively short time series and mainly focus on interdecadal climate variability (Jung et al., 2010; Jung et al., 2019; Miralles et al., 2013). Therefore, it is necessary to infer long-term ET from ground observations to reveal the dynamic changes in ET.

In this study, we employed an observation-driven, machine learning approach to estimate latent heat flux (λE) (ET in energy units) and sensible heat flux (H). This approach utilizes daily observations of temperatures, humidity, and solar radiation (Gentine et al., 2016). A major advantage is that the retrieval process is purely driven by observations; therefore, it does not rely on any assumptions of land processes (e.g., values of surface conductance), and it can represent the effects of dynamic changes in land surface conditions (Reichstein et al., 2019). Moreover, this approach allows for the monitoring of long-term changes in λE and H by accounting for shifting environmental conditions. In fact, λE dominates the moisture budget of the boundary layer, and H determines the growth of the boundary layer (Francesco et al., 2014; Gentine et al., 2011). The ratio of λE to the sum of λE and H, i.e., (EF), and a proxy for long-term runoff, i.e., precipitation (P) minus ET (P−ET), were also employed to quantify the surface aridity variability in this study.

https://doi.org/10.5194/hess-2020-590
Preprint. Discussion started: 21 November 2020

Hydrology and Earth System Sciences
Discussions
Open Access
EGU

2 Observational data and methodology

2.1 Flux tower observational data

We collected the half-hourly/hourly observational data and the integrated daily product from the FLUXNET2015 FULLSET dataset (Pastorello et al., 2020). To control the quality of the observational dataset, this study only used measurements and good-quality gap-filled data from 212 globally distributed flux towers (Supplementary Fig. S1a). The flux towers used in this study across various regions and land cover types (Fig. 1). The longest period of data availability is 22 years. This study intended to build a machine learning model for retrieving latent heat and sensible heat fluxes on a daily scale. Therefore, daily-scale data of top-of-atmosphere shortwave, vapor pressure deficit (VPD), mean temperature, and surface wind speed were collected from the integrated daily product of the FLUXNET2015. Daily maximum and minimum temperatures were obtained from half-hourly/hourly observational data. Data of daily λE and daily H were collected from the integrated daily product. The underlying surfaces of the flux towers covered different plant function types. According to the classification scheme of International Geosphere-Biosphere Programme, the plant function types include Evergreen Needleleaf Forest (ENF), Evergreen Broadleaf Forest (EBF), Deciduous Broadleaf Forest (DBF), Mixed Forest (MF), Croplands (CRO), Grasslands (GRA), Savannas (SAV), Woody Savannas (WSA), Open Shrublands (OSH), and Wetlands (WET).

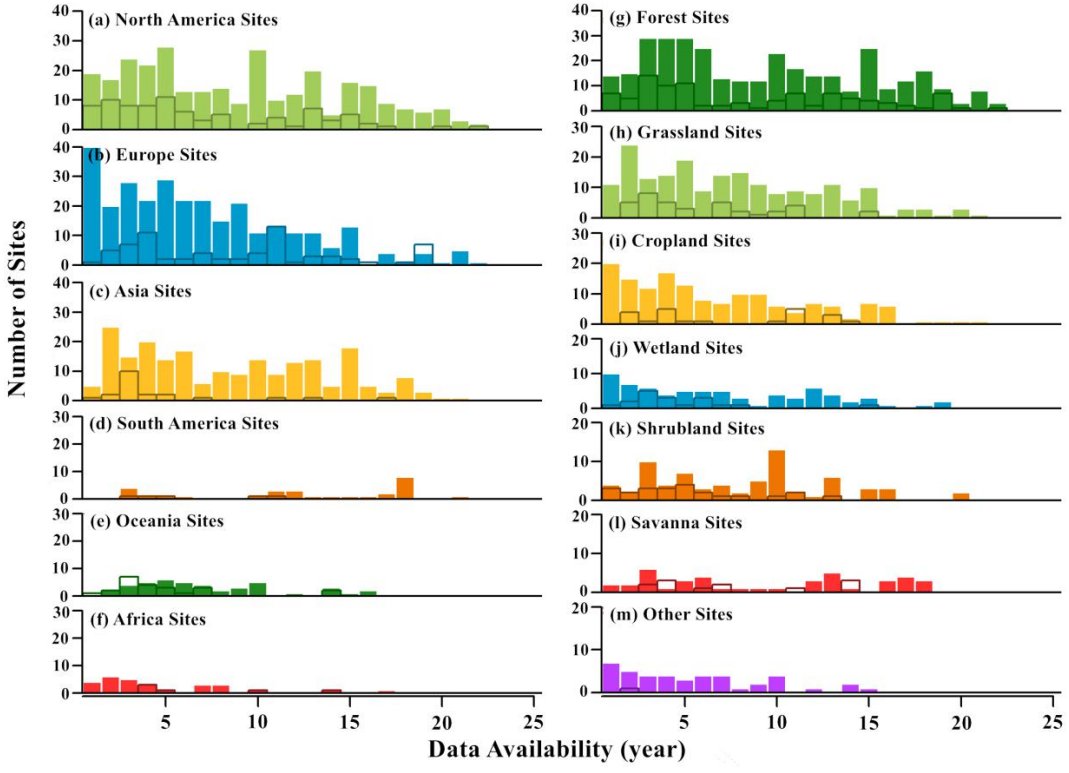

Figure 1. Data availability of the Fluxnet sites used in this study.

https://doi.org/10.5194/hess-2020-590
Preprint. Discussion started: 21 November 2020


Hydrology and Earth System Sciences
Discussions

2.2 Observational meteorological data

Daily meteorological observational records of precipitation (P), temperature (mean, maximum, and minimum temperatures), dew point temperature, and wind speed were collected from the Global Summary of the Day (GSOD) during the 1950–2017 period. The quality of the data was controlled through several procedures (Durre et al., 2010; Matsuura et al., 2009; Yin et al., 2018). Initially, we divided the weather stations into two groups: the original station group and target station group. We used 20 048 sites in total for the original station group (Supplementary Fig. S1b). Stations that had a time series span of less than ten years were excluded. The station records with the same geographic coordinates were merged into a single time series. When multiple sites were within the same 0.1-degree grid, we only selected one site for the target station group. After filtering, we obtained a total of 9835 stations for the target station group. In the subsequent spatiotemporal analysis, we only used weather stations with long-term data from the target station group.

Other procedures for controlling data quality were also implemented. Any implausible values, such as negative precipitation or a maximum temperature lower than the minimum temperature, were excluded. Monthly mean, maximum, and minimum temperatures, as well as precipitation were derived from daily observations at the original stations. Daily precipitation data were also compiled from records in the Global Historical Climatology Network (GHCN-Daily). The daily records of every weather station that had the same coordinates as the GHCN-Daily in the GSOD were compared, and the missing daily records were supplemented using the GHCN-Daily archives. Monthly data were calculated when the number of missing days within a month was no more than seven days. Additionally, missing monthly data from the target stations were interpolated from the original weather stations using the Kriging method in Python-based ArcGIS software.

2.3 Top-of-atmosphere shortwave radiation model

Daily top-of-atmosphere shortwave radiation converted from the hourly top-of-atmosphere shortwave radiation was forced to drive the ANN model for predicting the daily λE (H) at each of the target weather stations. The amount of incoming shortwave radiation at any location/time at the top-of-atmosphere was a function of Earth–Sun geometry, which has been defined as: i) latitude (i.e., location); ii) hour of day (due to the rotation of the earth); and iii) day of year (due to the tilted axis of the earth and its elliptical orbit around the sun). Several models for the top-of-atmosphere fluxes based on these inputs were available at varying levels of precision. The time-location model (Margulis, 2017) is shown as follows.

$$R_{s0} = \begin{cases} I_0 \dfrac{\cos\theta_0}{d^2}, & daytime : |\theta_0| \le 90^{\circ} \\ 0, & nighttime \end{cases} \quad (1)$$

where the cosine of the solar zenith angle is as follows:

$$\cos\theta_0 = \sin\delta \sin\lambda + \cos\delta \cos\lambda \cos\tau \quad (2)$$

https://doi.org/10.5194/hess-2020-590
Preprint. Discussion started: 21 November 2020


Hydrology and Earth System Sciences
Discussions

$$\delta = \frac{23.45\pi}{180} cos\left[\frac{2\pi}{365}(172 - DOY)\right] \quad (3)$$

$$\tau = 2\pi \frac{T_h - 12}{24} \quad (4)$$

$$d = 1 + 0.017 cos\left[\frac{2\pi}{365}(186 - DOY)\right] \quad (5)$$

Here, θ_0 is the solar zenith angle, δ is the declination angle, λ is latitude, τ is the hour angle, DOY represents the day of year, d represents the distance between the sun and Earth normalized by the mean distance, and T_h represents solar hour of the day.

2.4 Artificial neural network model training

A pure artificial neural network (ANN) was proven to have good performance in retrieving land surface fluxes, or in some cases, even better performance than that of hybrid models (Chen et al., 2020; Haughton et al., 2018; Zhao et al., 2019). In this study, we trained a multi-layer feedforward neural network model that consisted of an input layer, hidden layers, and an output layer to predict daily λE and H at the globally distributed weather stations. To identify the sensitivities of latent heat and sensible heat fluxes to different variables in the retrieval, ANN model was tested using different variable combinations as input (Supplementary Table S1). Top-of-atmosphere shortwave, relative humidity, surface wind speed, and the mean, maximum, and minimum temperatures were determined to be the inputs of the neural network (Supplementary Table S2). In the process of training ANN model, input data were randomly divided into three subsets using the percentages of 80%, 10%, and 10% for training, validation, and testing, respectively. The mean squared error (MSE) was used to evaluate the performance of the neural network in the process of adjusting weight. The root mean squared error (RMSE) and pearson correlation coefficient (R) between the predicted λE (H) and observed λE (H) were used to evaluate the retrieval performance of the trained ANN model. The neural network was determined to have two hidden layers and 15 neurons per hidden layer. A tangent sigmoid transfer function was used in the hidden layers, and a linear transfer function was used in the output layer. To avoid over-fitting, the training was stopped when the MSE could be reduced no further after traversing the entire dataset. The maximum number of training times and training accuracy goal were set to 500 epochs and 0.0001, respectively. Once one of the parameters exceeded the set threshold, model training was stopped.

2.5 EF linked to surface resistance (r_s) and aerodynamic resistance (r_a)

Here, we show that a long-term decline in EF can be strongly impacted by an increase in r_s. The latent heat flux is as follows.

https://doi.org/10.5194/hess-2020-590
Preprint. Discussion started: 21 November 2020


Hydrology and Earth System Sciences
Discussions

$$L_v E = L_v \rho \frac{e_{sat}(T_s) - e_a}{r_a + r_s} \tag{6}$$

where L_v is the latent heat of vaporization, E is evaporation flux, ρ is air density, T_s is near-surface air temperature, $e_{sat}(T_s)$ is saturated vapor pressure at the surface, e_a is actual air vapor pressure, r_a is aerodynamic resistance, and r_s is surface resistance. EF can be expressed as follows.

$$EF = \frac{L_v E}{L_v E + H} = \frac{L_v \rho \frac{e_{sat}(T_s) - e_a}{r_a + r_s}}{L_v \rho \frac{e_{sat}(T_s) - e_a}{r_a + r_s} + H} \tag{7}$$

We used the linearized Clausius–Clapeyron relation (Eq. (8) and Eq. (9)) to simplify Eq. (7).

$$e_{sat}(T_s) = e_{sat}(T_a) + \Delta(T_s - T_a) \tag{8}$$

$$T_s - T_a = \frac{H}{\rho c_p} \tag{9}$$

where T_a is the air temperature, $e_{sat}(T_a)$ is saturated vapor pressure of the air, and $\Delta = \frac{L_v}{R_v}\frac{e_s}{T^2}$, R_v is the gas constant for water vapor. Furthermore, c_p is the specific heat capacity, which is 4216 J kg^{-1} K^{-1} when the temperature is 0 °C.

$$EF = \frac{\frac{L_v \rho}{r_a + r_s}((e_{sat}(T_a) - e_a)) + \frac{\Delta H}{\rho c_p}}{\frac{L_v \rho}{r_a + r_s}((e_{sat}(T_a) - e_a)) + H} \tag{10}$$

$$= \frac{\frac{L_v \rho}{r_a + r_s}\left\{VPD + \frac{\Delta H}{\rho c_p}\right\}}{\frac{L_v \rho}{r_a + r_s}\left\{VPD + \frac{\Delta H}{\rho c_p}\right\} + H} \tag{11}$$

$$= \frac{1}{1 + \frac{r_a + r_s}{L_v \rho(\frac{\Delta}{\rho c_p} + \frac{VPD}{H})}} \tag{12}$$

The incremental variation of $\frac{VPD}{H}$ is small because both variations of VPD and H are proportional to the temperature variation. EF can be expressed as follows:

https://doi.org/10.5194/hess-2020-590
Preprint. Discussion started: 21 November 2020


Hydrology and Earth System Sciences
Discussions

$$\frac{1}{EF} = 1 + \frac{r_a + r_s}{\frac{L_v}{c_p}\Delta} \tag{13}$$

Hence, r_s is a function of EF.

$$r_s = \frac{L_v}{c_p}\Delta\left(\frac{1}{EF} - 1\right) - r_a \tag{14}$$

A decline in the EF can be induced by an increase in the surface resistance, r_s. Annual EF ranged from 0 to 1, and the variations in EF (ΔEF) were closely related to plant physiological effects. The range of influence from r_a on ΔEF was relatively small, while the range of influence from r_s on ΔEF was relatively larger.

3 Results and discussion

3.1 ANN model retrievals

Cross-validations of the ANN model were first performed. Taking one set of cross-validation as an example, the correlation coefficient (R) between the predicted daily λE and the observed daily λE is 0.782 and the R between the predicted daily H and the observed daily H is 0.768, and both the correlations are significant at the p<0.001 level (Fig. 2). Furthermore, the ANN model was cross-validated in different verification sets whose samples were randomly selected from a type of plant function type (Supplementary Fig. S2). The abilities of the trained ANN model for predicting latent heat and sensible heat fluxes were different for various plant function types. With the exception of OSH (R = 0.680, p < 0.05), the R of the daily-scale λE of DBF, MF, SAV, GRA, CRO, and WET were all greater than 0.80, and all correlation coefficients were statistically significant at the p < 0.001 level. A common feature of these plant function types was that they belonged to the ecosystems with relatively open bodies of water or high vegetation coverage, while the water transfer of OSH from the land to the atmosphere was easily limited by soil moisture. Therefore, the R for OSH was relatively low (R = 0.656) and this is because the total evapotranspiration in OSH is mainly controlled by the evaporation process which is easily restricted by the soil water supply capacity; however, the correlation was also significant at the p < 0.05 level. With respect to the estimation of daily H, the R of estimating H in other plant function types was greater than 0.716, and all were statistically significant at the 0.001 level. In addition, the trained ANN model also shows good simulation ability under some other ecosystems with relatively sparse vegetation cover such as savannas (SAV), grasslands(GRA), croplands(CRO), and wetlands(WET) (Supplementary Fig. S3). In summary, in addition to OSH, the accuracy of retrieving λE is high in GRA, CRO, WET, and various forest ecosystems, and these ecosystems were characterized by sufficient water supply or dense vegetation cover. For the estimation of H, except for the estimation of H in farmland, the correlations of predicted and observed H in all ecosystems are correlated at the p < 0.001 level, especially in forest ecosystems. It needs to be emphasized that the

https://doi.org/10.5194/hess-2020-590
Preprint. Discussion started: 21 November 2020

Hydrology and Earth System Sciences
Discussions

magnitude of R could be affected by the number of samples, and the sample number of each verification set in the cross-validations is large (n > 12 000).

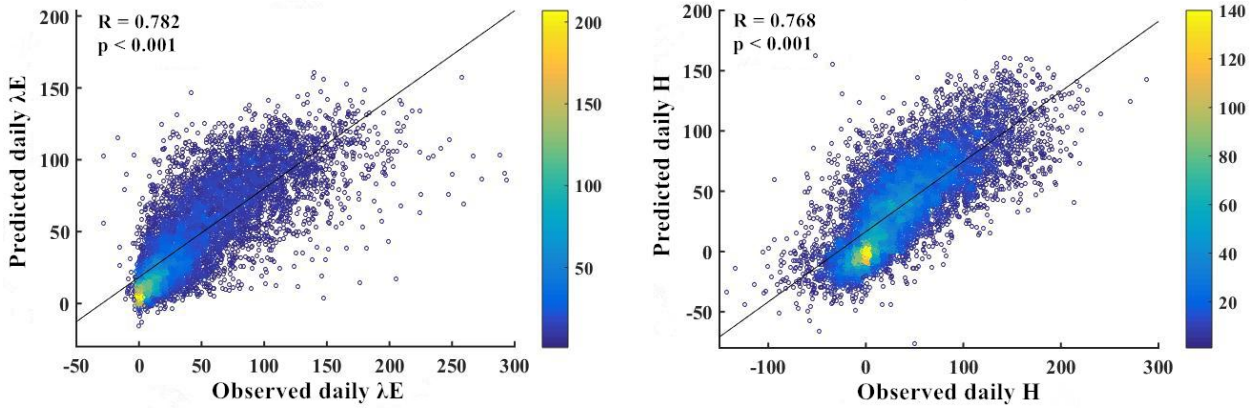

Figure 2. Density scatter plot of the cross-validation. Samples of five flux towers were randomly retained as verification set.

The uncertainty and bias characteristics of the ANN model retrievals were further analyzed on both daily and monthly scales. On the daily scale, the correlation coefficients between predicted λE (verse H) and observed λE (verse H) were 0.78~0.79 (0.77~0.78) ($p < 0.001$) (Supplementary Fig. S4). The RMSE of λE (H) ranged from 26.05 to 26.32 W m^{-2} (28.61 to 29.15 W m^{-2}). More than 80% of the 212 flux towers had a correlation greater than 0.70. As for the RMSE, 85% and 89% of the daily λE (H) were less than 30 W m^{-2}, respectively. It was obvious that flux towers with large biases were mainly located on the coast of Australia and the west coast and Great Lakes region of the United States, as well as the Mediterranean region, all of which are strongly impacted by advection from neighboring bodies of open water. The bias of the monthly scale estimates was smaller than that of the daily scale estimates. More than 89% and 90% of the sites had an R greater than 0.70 (Supplementary Fig. S5). Meanwhile, more than 88% and 89% of the sites showed an RMSE of less than 30 W m^{-2} in λE and H, respectively. Similar to the spatial distribution of biases on a daily scale, flux towers with large biases were located on the coast of Australia, the Great Lakes region, and the Mediterranean region. Finally, global daily-scale latent heat and sensible heat fluxes were predicted by the ANN model. The spatial distributions of mean annual λE and H were shown in Supplementary Fig. S6. The mean annual ET in the FLUXCOM ranged from 0 to 1400 mm (Jung et al., 2010), while the mean annual ET of this study ranged from 0 to 1416 mm during the 1982−2008 period (Supplementary Fig. S7). In different large-scale latitude intervals, the temporal changes of λE estimated by the ANN and λE in the FLUXCOM are significantly correlated at the $p < 0.05$ (Supplementary Fig. S8). This study were primarily concerned with the direction and magnitude of long-term trends, and thus, relative bias could be tolerated.

3.2 Attribution of trends in climate variables

https://doi.org/10.5194/hess-2020-590
Preprint. Discussion started: 21 November 2020

Hydrology and Earth System Sciences
Discussions

The trends in climate variables were estimated for two reasons: (1) to quantify the changes in the atmospheric water supply, and (2) to estimate the trends in VPD, air temperature, and wind speed to understand the characteristics of changes in atmospheric evaporative demand. The annual precipitation exhibited increasing trends ranging from 3 to 40 mm per decade in western Europe, the United States, Southeast Asia, and Australia. Meanwhile, the annual precipitation exhibited decreasing trends, mainly ranging from -3 to -30 mm per decade in the northern Eurasian continent, savanna region of Brazil, and South Africa (Fig. 3a). Especially in recent 2001–2017 period, precipitation has shown a more obvious upward trend than before in a wide area of the global land (Supplementary Fig. S9). Increases in air temperature and the water holding capacity of the atmosphere were the primary causes for the significant increase in precipitation (Byrne et al., 2015), except for certain regions (e.g., Russia) with insufficient moisture advection from an ocean or regional ET.

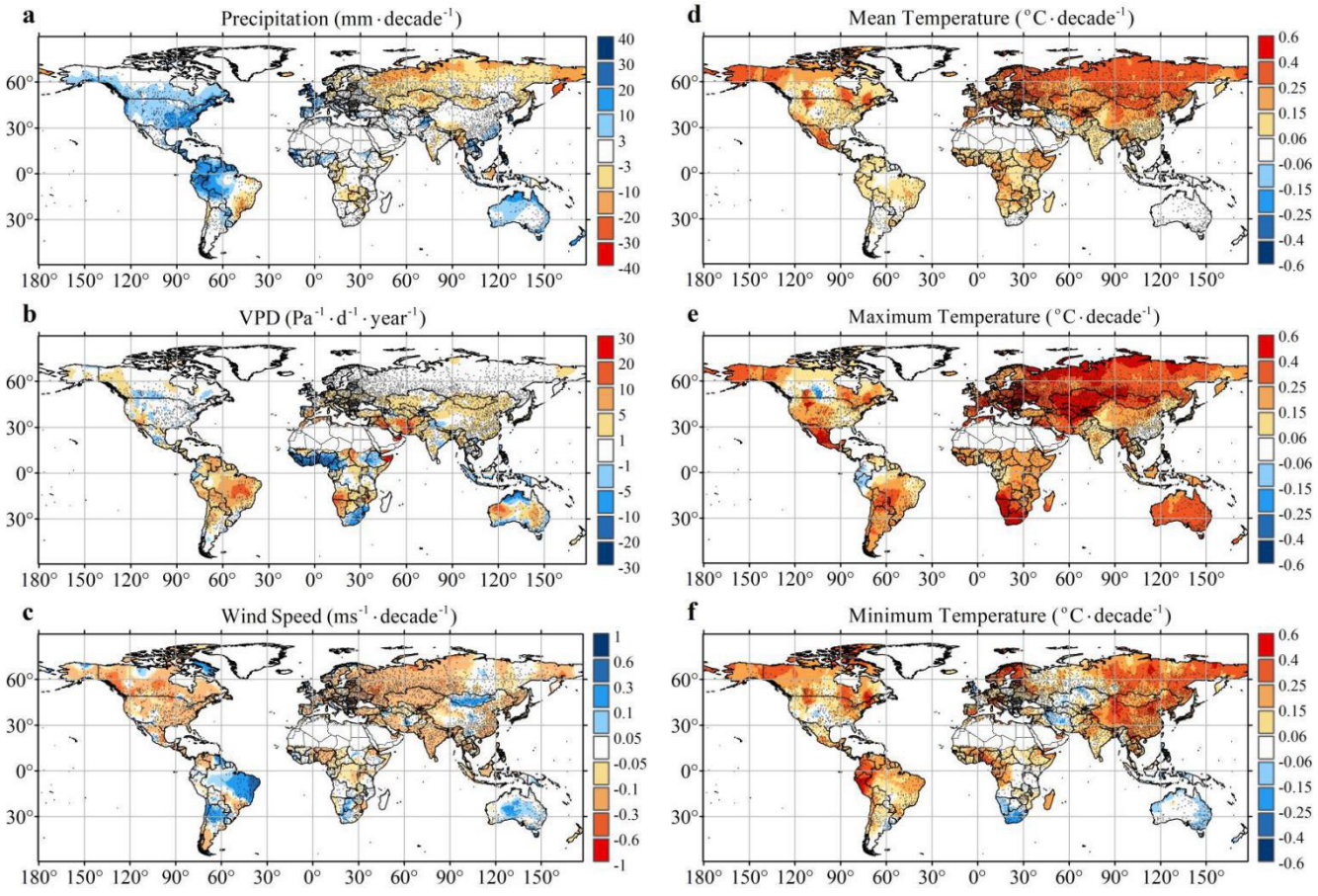

Figure 3. Long-term trends in annual precipitation, vapor pressure deficit (VPD), wind speed, mean temperature, maximum temperature, and minimum temperature. Values are not shown for Greenland or Sahara Desert. Small gray squares show locations of weather stations used to interpolate global patterns.

https://doi.org/10.5194/hess-2020-590
Preprint. Discussion started: 21 November 2020


Hydrology and Earth System Sciences
Discussions

With respect to the side of atmospheric water demand, the VPD primarily presented an increasing trend because of an increase in air temperature and a decrease in relative humidity, especially in the subtropics; this was consistent with the expectations of atmospheric dynamics and the influence of free-tropospheric warming (Fig. 3b). Additional variables influencing the evaporative demand, such as the mean, maximum, and minimum temperatures, mostly presented increasing trends on the global scale, with the exception of a few areas, such as the United States/Canadian Corn Belt, Mexico, and northern Europe, which showed signs of cooling due to land use management such as agricultural irrigation (Thiery et al., 2017) (Fig. 3d−f). Therefore, both rising air temperatures and increased VPD under climate warming indicate a trend of increasing drag force of evaporation and transpiration. In addition, the mean surface wind speed—a meteorologic factor associated with evaporation—showed an overall decreasing trend (i.e., global stilling) except in the Amazon, Argentina, Australia, and Mongolia (Fig. 3c).

3.3 Long-term trends in EF, ET, and P–ET

When the annual EF ranges from 0 (full aridity stress) to 1 (no aridity stress), it is an indicator of surface aridity linked to soil moisture availability and vegetation phenology, as well as the physiological effects of CO_2 on vegetation (Francesco et al., 2014; Lemordant et al., 2018; Swann et al., 2016). The decreasing trend in the EF varied from 0 to 0.05 per decade and was prevalent in several land areas (Fig. 4a), except in areas with the most humid tropical rainforests (i.e., the Amazon, West Africa, New Guinea Island, and Southeast Asia) and dense agricultural irrigation areas, including central North America and Punjab in India (Supplementary Fig. S10). Changes in the EF at different latitudinal intervals were consistent with the "dry gets drier, wet gets wetter" paradigm in the tropical areas (Chou et al., 2009; Liu et al., 2013). The observed increase in EF further suggested a wet trend in the western Sahel, where an increase in rainfall was reported recently (Biasutti, 2019; Dong et al., 2015). It was systematically determined that the EF has declined across large swaths of the globe over the past several decades, which emphasized that this is a persistent long-term trend, not a short-term phenomenon (Fig. 5a–c). As the climate has warmed, a decrease in the EF reflected an increase in surface resistance (see Methodology), which can be controlled by one of two factors—either an increase in stomatal resistance associated with the physiological effects of CO_2 or a decrease in soil moisture. Therefore, if we find that soil moisture or surface runoff increases while the EF decreases, this is a signal that surface resistance has increased.

The evolution of El Niño–Southern Oscillation (ENSO) can greatly influence the global hydrological cycle and patterns of aridity/wetness (Miralles et al., 2013; Nalley et al., 2019), and thus we analyzed the patterns of EF in different ENSO phases based on the multivariate ENSO index (MEI). However, no significant changes in EF trends were detected between different ENSO phases, with the exception of La Niña having a significant impact on the aridity in East Asia (Fig. 5d–f). The EF simulated by Earth System Models under the RCP8.5 scenario (the scenario with the highest CO_2 emissions) also presented a decreasing trend in most global land areas, even if the trend in the models appeared to be stronger than that of the trend

https://doi.org/10.5194/hess-2020-590
Preprint. Discussion started: 21 November 2020

Hydrology and Earth System Sciences
Discussions

estimated by the data-driven EF (Fig. 6a). This further suggested that increasing CO_2 concentrations have an impact on the EF, and the observed decrease in EF was consistent with that of the prediction of the model. However, the climate model missed several areas where agricultural practices led to an increase in EF, as well as in the tropical rainforest where there
250 was a deviation in peak precipitation (Yin et al., 2013).

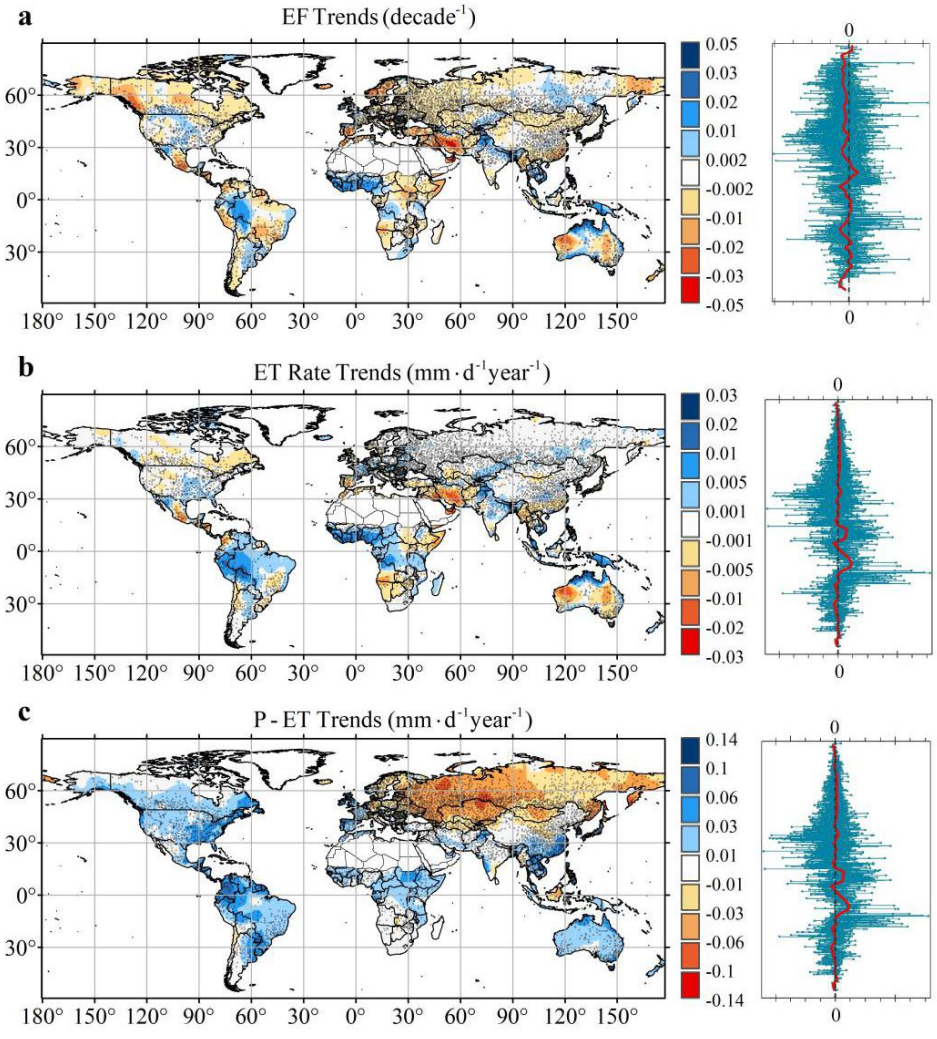

Figure 4. Long-term trends in evaporative fraction (EF), evapotranspiration (ET), and precipitation (P) minus ET (P−ET). Daily ET is converted from daily latent heat flux retrieved by ANN model. Red curve represents median variation of different latitudes.

255 As the climate has warmed, the ET has shown a significant increasing trend, ranging from 0 to 0.03 mm per day per year (Fig. 4b), especially in the main regions with tropical rainforests (e.g., the Amazon, West Africa, and Southeast Asia), the coast of Australia, and areas with a high density of agricultural irrigation (e.g., northern India, Central Asia, and Central

https://doi.org/10.5194/hess-2020-590
Preprint. Discussion started: 21 November 2020

Hydrology and Earth System Sciences
Discussions

America). The increase in ET was primarily induced by the radiative effect of a warming climate, which could compensate for the observed decrease in EF ($ET = EF \times R_n$). Signs of decline in ET at a rate of 0 to -0.03 mm per day per year were found on fractional land surfaces, such as North America, South Africa, and the Mediterranean, which was consistent with the predictions made by the RCP8.5 climate model (Fig. 6b).

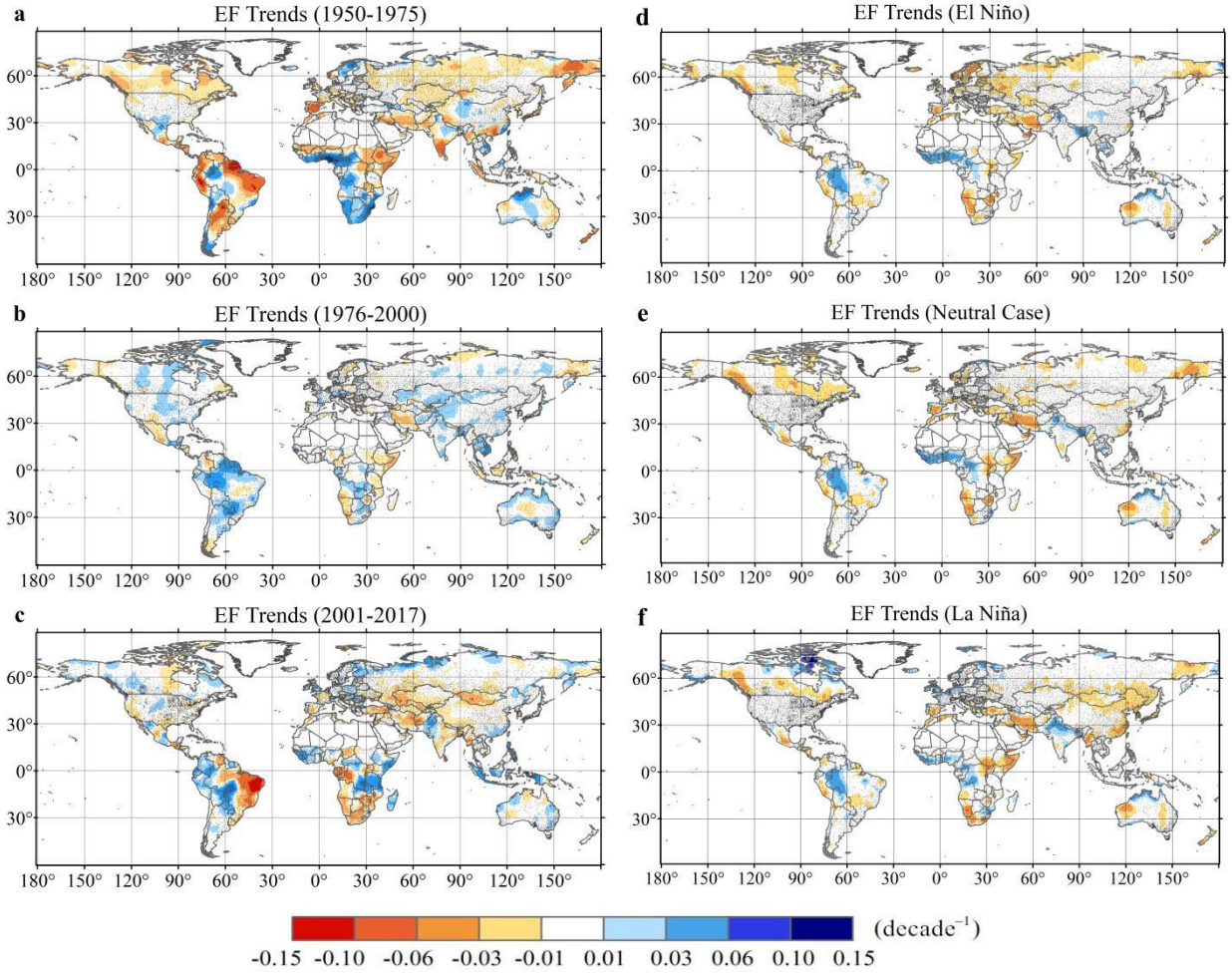

Figure 5. Spatial patterns of EF trends during different periods. (a–c) EF trends during various historical periods. (d–f) EF trends during El Niño period, a neutral case, and La Niña period, respectively.

P−ET, a proxy for long-term runoff, assumes that changes in storage due to human activity are negligible and are closely linked to water availability and soil moisture trends (Alkama et al., 2013; Sophocleous et al., 2002). Therefore, long-term runoff presented a significant increasing trend, with the exception of a decrease in northern Eurasia (Fig. 4c). To further verify the retrieved P–ET trend, we compared the P–ET trend with the observed runoff trend during the same periods in small- to medium-sized watersheds (5~1000 km^2) (Supplementary Fig. S11). The P–ET and observed runoff presented

https://doi.org/10.5194/hess-2020-590
Preprint. Discussion started: 21 November 2020

Hydrology and Earth System Sciences
Discussions

different trends in eastern Australia, which could be attributed to a decrease in runoff caused by human activities because there are clusters of cities in this area where the observed runoff was strongly affected by human activities (Bosmans et al., 2017). Nevertheless, similarities could also be found in the P–ET and observed runoff trends. In western Europe and eastern North America, both the P–ET and observed runoff showed an increasing trend, and both the Mediterranean region and South Africa showed a decreasing trend. The RCP8.5 model also predicted an overall increasing trend in P−ET (Fig. 6c), while a decrease was predicted (but not observed) in the western United States and western Europe. Additionally, an increased P−ET was predicted (but not widely observed) in northern Eurasia.

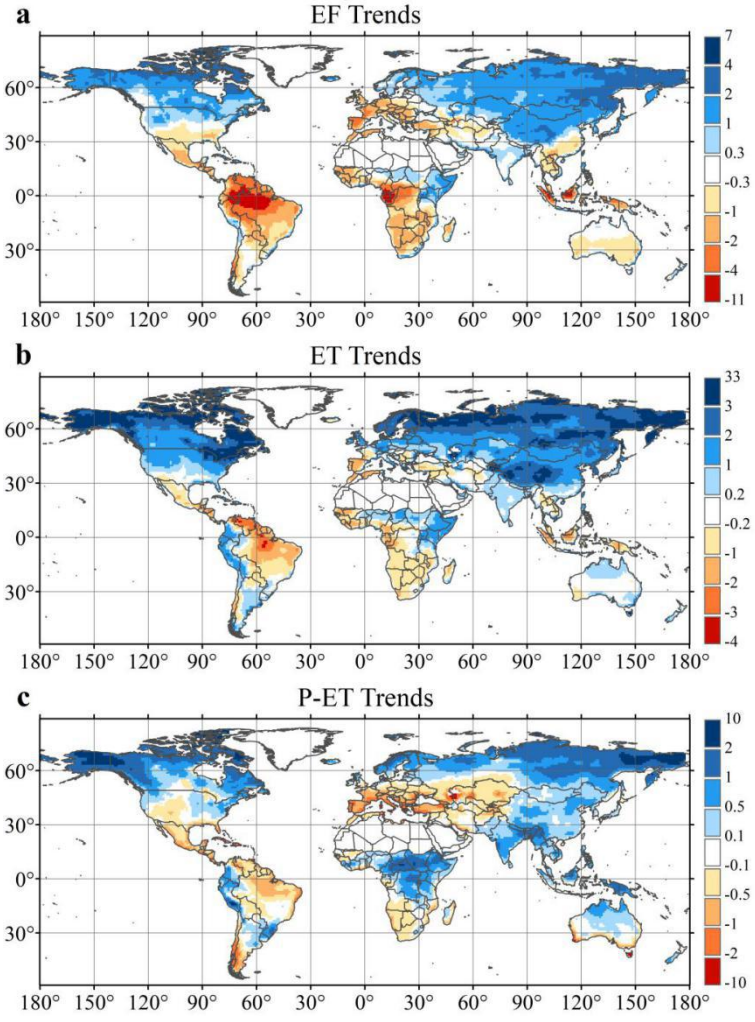

Figure 6. Annual changes in (a) EF, (b) ET, and (c) P−ET in CMIP5 RCP 8.5 Earth System Models with all anthropogenic forcing (e.g., land use and land cover changes, aerosols, and ozone). Changes are quantified by difference in years 2070−2099 of simulation and years 1941−1970.

https://doi.org/10.5194/hess-2020-590
Preprint. Discussion started: 21 November 2020

Hydrology and Earth System Sciences
Discussions

3.4 Signs of covariation in long-term EF and runoff

The signs of covariation in normalized ET, i.e., EF, and normalized P−ET, i.e., 1−ET/P, were further investigated to determine the patterns of surface aridity. We superimposed the EF trend, indicative of changes in aridity stress (e.g., temperature and soil moisture) or plant physiological effects (see Methodology), and the 1−ET/P trend, which was indicative of changes in long-term runoff. Land areas with a decreased EF and an increased long-term 1−ET/P were indicative of significant plant physiological effects of CO_2. This was because a long-term relative decline in ET with increasing runoff was mainly attributed to plant physiological control. A decline in the EF caused by a decrease in surface conductance could be offset by an increase in the EF caused by the effects of climate warming. Nevertheless, in 27.06% of the global land areas, the EF has declined and has been accompanied by an increase in long-term runoff, which has been observed in most of North America, parts of South America, the Mediterranean, Africa, Australia, and Southeast China (Fig. 7). These signals further emphasized that surface vegetation and its response to a changing environment have a great influence on water cycle regulation and surface aridity variability.

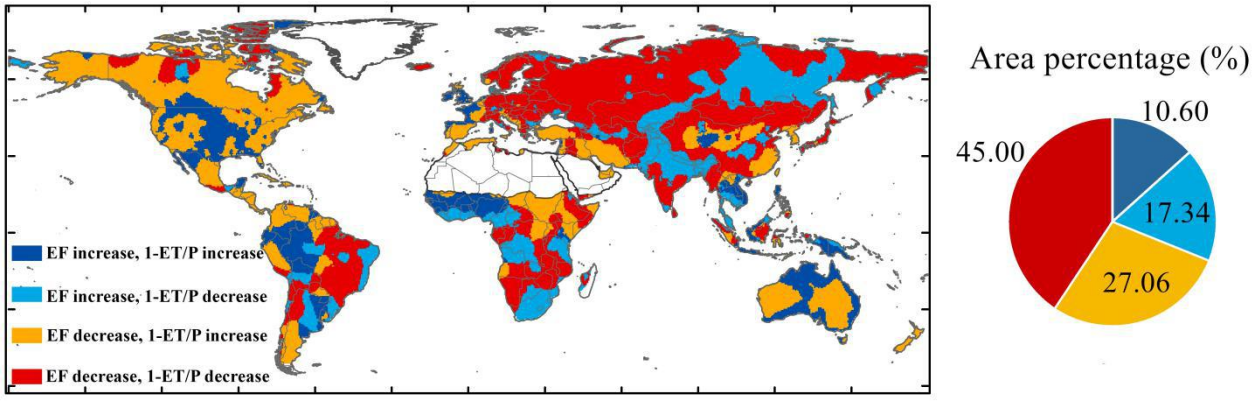

Figure 7. Signs of covariation in EF and 1–ET/P. Right panel shows area percentage of different signs.

In addition, an increase in the EF was accompanied by a long-term decrease in runoff, which accounted for 17.34% of the land areas, which was mainly due to changes in agricultural irrigation and land use management in places such as Punjab in India, Central Asia, and downstream Amazon where there is a high density of irrigation. The land areas in which both the EF and long-term runoff had an increasing trend were typically located in humid regions and accounted for 10.60% of the land surface area. With an increase in the EF and 1–ET/P, the humid areas of the Amazon, West Africa, Southeast Asia, and the coast of Australia have become increasingly wet (Fig. 7). The wet trend in the western Sahel was also captured by the increases in both EF and 1–ET/P. Additionally, 45.00% of the global land areas showed a decreasing trend in EF and 1−ET/P, and aridity stress posed a larger risk to these regions. In the arid regions of the Amazon, (e.g., the savanna region of Brazil), the EF and 1–ET/P both exhibited a decreasing trend that corresponded with an arid trend. The Mediterranean region,

https://doi.org/10.5194/hess-2020-590
Preprint. Discussion started: 21 November 2020

305 northern Eurasia, and South Africa were also expected to become more arid, which was consistent with existing aridity observations and predictions (Padrón et al., 2020; Samaniego et al., 2018; Zhou et al., 2019).

4 Summary

This study provided a strategy for retrieving large-scale ET, as well as provided a quantification of the changes in surface aridity/wetness using machine learning approach driven by ground observations from globally distributed flux towers and 310 weather stations. The results had important implications for understanding changes in surface aridity and provided constraints for future climate model predictions. Although we attempted to infer latent heat and sensible heat fluxes from in situ ground observations and used various data quality control methods to reduce uncertainty, the quality of the observational data from the flux towers and weather stations could have influenced the retrievals.

315 In the absence of surface regulation of plant physiological effect and changes in biomass, a warming climate was expected to intensify ET at a rate roughly governed by the Clausius–Clapeyron relation. However, a long-term relative decrease in normalized ET accompanied by increasing runoff was found in 27.06% of the global land areas, which was indicative of a reduction in surface conductance. The findings in this study further emphasized that vegetation controls have strong impacts in regulating the water cycle and surface aridity variability. Climate models have captured some of these changes; however, 320 they have also exhibited large regional discrepancies. Therefore, representations of land use management and plant physiological effects are essential for improved future predictions with respect to the water, energy, and carbon cycles.

325 *Data/code availability.* The data and codes of each step in this study is available upon request. The eddy-covariance data are available at http://fluxnet.fluxdata.org/. The Global Summary of the Day and the Global Historical Climatology Network datasets are collected from the NOAA at https://www.ncdc.noaa.gov/data-access. The data of Global Runoff Data Center are available at https://www.bafg.de/GRDC/EN/01_GRDC/13_dtbse/database_node.html. Global irrigation data are available at http://www.fao.org/nr/water/aquastat/irrigationmap/index10.stm. The Multivariate ENSO Index (MEI) is available at 330 https://www.esrl.noaa.gov/psd/enso/mei/.

Author contributions. RW and PG designed the study. RW performed the experiment and wrote the manuscript. PG designed the methodology, analyzed the results, and revised the manuscript. JY and LC contributed to data curation and validation. JC and LL contributed to discussion and supervision.

335

Competing interests. The authors declare that they have no conflict of interest.

Acknowledgments. We acknowledge the members of FLUXNET community for sharing flux tower observational data.

Financial support. This work was founded by the National Key Research and Development Program of China (2017YFA0603603) and the China Postdoctoral Science Foundation (2020M681656).

References

Alkama, R., Marchand, L., Ribes, A., and Decharme, B.: Detection of global runoff changes: results from observations and CMIP5 experiments, Hydrol. Earth Syst. Sci., 17, 2967–2979, https://doi.org/10.5194/hess-17-2967-2013, 2013.

Baruga, C. K., Kim, D., Choi, M.: A national-scale drought assessment in Uganda based on evapotranspiration deficits from the Bouchet hypothesis. J. Hydrol., 580:124348, https://doi.org/10.1016/j.jhydrol.2019.124348, 2020.

Berg, A., Findell, K., Lintner, B., et al.: Land-atmosphere feedbacks amplify aridity increase over land under global warming. Nat. Clim. Change, 6, 869–874, https://doi.org/10.1038/nclimate3029, 2016.

Biasutti, M.: Rainfall trends in the African Sahel: Characteristics, processes, and causes. WIREs Clim. Change, 10: e591, https://doi.org/10.1002/wcc.591, 2019.

Bosmans, J. H. C., van Beek L. P. H., Sutanudjaja, E. H., Bierkens M. F. P.: Hydrological impacts of global land cover change and human water use. Hydrol. Earth Syst. Sci., 21: 5603–5626, https://doi.org/10.5194/hess-21-5603-2017, 2017.

Byrne, M. P., O'Gorman, P. A.: The response of precipitation minus evapotranspiration to climate warming: Why the "wet-get-wetter, dry-get-drier" scaling does not hold over land. J. Clim., 28, 8078–8092, https://doi.org/10.1175/JCLI-D-15-0369.1, 2015.

Chen, Z. J., Zhu, Z. C., Jiang, H., Sun S. J.: Estimating daily reference evapotranspiration based on limited meteorological data using deep learning and classical machine learning methods. J. Hydrol., 591, 125286, https://doi.org/10.1016/j.jhydrol.2020.125286, 2020.

Chou, C., Neelin, J. D., Chen, C. A., Tu, J. Y.: Evaluating the "rich-get-richer" mechanism in tropical precipitation change under global warming. J. Clim., 22, 1982–2005, https://doi.org/10.1175/2008JCLI2471.1, 2009.

Cook, B. I., Smerdon, J. E., Seager, R., Coats, S.: Global warming and 21st century drying. Clim. Dyn., 43(9-10), 2607–2627, https://doi.org/10.1007/s00382-014-2075-y, 2014.

Costa, M. H., Biajoli, M. C., Sanches, L., Malhado, A. C. M., Hutyra, L. R., da Rocha, H. R., Aguiar, R. G., and de Araújo, A. C.: Atmospheric versus vegetation controls of Amazonian tropical rain forest evapotranspiration: Are the wet and seasonally dry rain forests any different?, J. Geophys. Res.: Biogeo., 115, G04021, https://doi.org/10.1029/2009jg001179, 2010.

https://doi.org/10.5194/hess-2020-590
Preprint. Discussion started: 21 November 2020

370 Dai, A.: Increasing drought under global warming in observations and models. Nat. Clim. Change, 3(2), 171–171, https://doi.org/10.1038/nclimate1633, 2013.

Durre, I., Menne, M. J., Gleason, B. E., Houston, T. G., Vose, R. S.: Comprehensive automated quality assurance of daily surface observations. J. Appl. Meteorol. Clim., 49, 1615–1633, https://doi.org/10.1175/2010JAMC2375.1, 2010.

Dong, B., Sutton, R.: Dominant role of greenhouse-gas forcing in the recovery of Sahel rainfall. Nat. Clim. Change, 5, 757–
375 760, https://doi.org/10.1038/nclimate2664, 2015.

Forzieri, G., Gonzalez, Miralles D., et al.: Increased control of vegetation on global terrestrial energy fluxes. Nat. Clim. Change 10, 356–362, https://doi.org/10.1038/s41558-020-0717-0, 2020.

Fu, Q. and Feng, S.: Responses of terrestrial aridity to global warming. J. Geophys. Res.: Atmos. 119(13), 7863–7875, https://doi.org/10.1002/2014JD021608, 2014.

380 Francesco, N., Mirco, B., Gabriele, C., Stefano, B. and Pietro, B.: Evaporative fraction as an indicator of moisture condition and water stress status in semi-arid range land ecosystems. Remote Sens., 6(7), 6300–6323, https://doi.org/10.3390/rs6076300, 2014.

Gentine, P., Chhang, A., Rigden, A. and Salvucci, G.: Evaporation estimates using weather station data and boundary layer theory. Geophys. Res. Lett. 43, 11661–11670, https://doi.org/10.1002/2016GL070819, 2016.

385 Gentine, P., Entekhabi, D. and Polcher, J.: The diurnal behavior of evaporative fraction in the soil-vegetation-atmospheric boundary layer continuum. J Hydrometeorol., 12, 1530–1546, https://doi.org/10.1175/2011JHM1261.1, 2011.

Greve, P., Orlowsky, B., Mueller, B., Sheffield, J., Reichstein, M. and Seneviratne, S. I.: Global assessment of trends in wetting and drying over land. Nat. Geosci., 7(10), 716–721, https://doi.org/10.1038/ngeo2247, 2014.

Hoek van Dijke, A. J., Mallick, K., Schlerf, M., Machwitz, M., Herold, M. and Teuling, A. J. Examining the link between
390 vegetation leaf area and land–atmosphere exchange of water, energy and carbon fluxes using FLUXNET data. Hydrol. Earth Syst. Sci., 17: 4443–4457, https://doi.org/10.5194/bg-17-4443-2020, 2020.

Jaramillo, F., Cory, N., Arheimer, B., Laudon, H., van der Velde, Y., Hasper, T. B., Teutschbein, C. and Uddling, J: Dominant effect of increasing forest biomass on evapotranspiration: interpretations of movement in Budyko space. Hydrol. Earth Syst. Sci., 22: 567–580, https://doi.org/10.5194/hess-22-567-2018, 2018.

395 Jung, M., Reichstein, M., Ciais, P., Seneviratne, S.I., Sheffield, J., et al.: Recent decline in the global land evapotranspiration trend due to limited moisture supply. Nat. 467, 951–954, https://doi.org/10.1038/nature09396, 2010.

Jung, M., Koirala S., Weber U., Ichii, K., Gans, F., Camps-Valls G., Papale, D., Schwalm, C. R., Tramontana and G., Reichstein, M.: The FLUXCOM ensemble of global land-atmosphere energy fluxes. Sci. Data., 6, 74, https://doi.org/10.1038/s41597-019-0076-8, 2019.

400 Keenan, T. F., Hollinger, D. Y., Bohrer, G., Dragoni, D., Munger, J. W., Schmid, H. P. and Richardson A. D.: Increase in forest water-use efficiency as atmospheric carbon dioxide concentrations rise. Nat., 499(7458), 324–327, https://doi.org/10.1038/nature12291, 2013.

https://doi.org/10.5194/hess-2020-590
Preprint. Discussion started: 21 November 2020

Komatsu, H. and Kume, T.: Modeling of evapotranspiration changes with forest management practices: A genealogical review. J. Hydrol., 585, 124835, https://doi.org/10.1016/j.jhydrol.2020.124835, 2020.

Lemordant, L., Gentine, P., Swann, A. S., et al.: Critical impact of vegetation physiology on the continental hydrologic cycle in response to increasing CO_2. Proc. Natl. Acad. Sci. USA, 16, 4093–4098, https://doi.org/10.1073/pnas.1720712115, 2018.

Liu, C. and Allan, R. P.: Observed and simulated precipitation responses in wet and dry regions 1850–2100. Environ. Res. Lett. 8(3), 034002, https://doi.org/10.1088/1748-9326/8/3/034002, 2013.

Mallick, K., Trebs, I., Boegh, E., Giustarini, L., Schlerf, M., Drewry, D. T., Hoffmann, L., Von Randow, C., Kruijt, B., Araùjo, A., Saleska, S., Ehleringer, J. R., Domingues, T. F., Ometto, J. P. H. B., Nobre, A. D., Luiz Leal De Moraes, O., Hayek, M., William Munger, J., and Wofsy, S. C.: Canopy-scale biophysical controls of transpiration and evaporation in the Amazon Basin, Hydrol. Earth Syst. Sci., 20, 4237–4264, https://doi.org/10.5194/hess-204237-2016, 2016.

Margulis, S. A., 2017. Introduction to hydrology, https://margulis-group.github.io/teaching/.

Massmann, A., Gentine, P., Lin, C.: When does vapor pressure deficit drive or reduce evapotranspiration?. J. Adv. Model. Earth Sy. 11(10): 3305-3320, https://doi.org/10.1029/2019MS001790, 2019.

Miralles, D. G., DeJeu, R. A. M., Gash, J. H., Holmes, T. R. H., and Dolman, A. J.: Magnitude and variability of land evaporation and its components at the global scale, Hydrol. Earth Syst. Sci., 15, 967–981, https://doi.org/10.5194/hess-15-967-2011, 2011.

Miralles, D. G., Van, d. B. M. J., Gash, J. H., et al.: El Niño–La Niña cycle and recent trends in continental evaporation. Nat. Clim. Change 4(2), 122–126, https://doi.org/10.1038/nclimate2068, 2013.

Miralles, D. G., Brutsaert, W., Dolman, A. J., and Gash, J. H.: On the use of the term “evapotranspiration”. Water Resour. Res. 56, e2020WR028055, https://doi.org/10.1029/2020WR028055, 2020.

Milly, P. C., Dunne, K. A.: Potential evapotranspiration and continental drying. Nat. Clim. Change, 6, 946–949, https://doi.org/10.1038/nclimate3046, 2016.

Nalley, D., Adamowski, J., Biswas, A., Gharabaghi, B., Hu, W.: A multiscale and multivariate analysis of precipitation and streamflow variability in relation to ENSO, NAO and PDO. J. Hydrol., 574: 288–307, https://doi.org/10.1016/j.jhydrol.2019.04.024, 2019.

Naumann, G., Alfieri, L., Wyser, K., et al.: Global changes in drought conditions under different levels of warming. Geophys. Res. Lett. 45, 3285–3296, https://doi.org/10.1002/2017GL076521, 2018.

Ned, H., Gab, A., Pitman, A. J.: On the predictability of land surface fluxes from meteorological variables. Geosci. Model Dev. 11(1), 195–212, https://doi.org/10.5194/bg-15-4495-2018, 2018.

Padrón, R. S., Gudmundsson, L., Decharme, B., et al.: Observed changes in dry-season water availability attributed to human-induced climate change. Nat. Geosci. 2020, 13(7): 477–481, https://doi.org/10.1038/s41561-020-0594-1, 2020.

Pastorello, G., Trotta, C., Canfora, E. et al.: The FLUXNET2015 dataset and the ONEFlux processing pipeline for eddy covariance data. Sci. Data 7, 225, https://doi.org/10.1038/s41597-020-0534-3, 2020.

https://doi.org/10.5194/hess-2020-590
Preprint. Discussion started: 21 November 2020

Reichstein, M., Camps-Valls, G., Stevens, B., et al.: Deep learning and process understanding for data-driven Earth system science. Nat. 566, 195, https://doi.org/10.1038/s41586-019-0912-1, 2019.

Rigden, A. J., Salvucci, G. D.: Evapotranspiration based on equilibrated relative humidity (ETRHEQ): Evaluation over the continental US. Water Resour. Res. 51, 2951–2973, https://doi.org/10.1002/2014WR016072, 2015.

Rigden, A. J., Salvucci, G. D.: Stomatal response to humidity and CO_2 implicated in recent decline in US evaporation. Global Change Biol. 23(3), 1140–1150, https://doi.org/10.1111/gcb.13439, 2016.

Salvucci, G. D., Gentine, P.: Emergent relation between surface vapor conductance and relative humidity profiles yields evaporation rates from weather data. Proc. Natl. Acad. Sci. USA 110, 6287–6291, https://doi.org/10.1073/pnas.1215844110, 2013.

Samaniego L, Thober S, Kumar R, et al: Anthropogenic warming exacerbates European soil moisture droughts. Nat. Clim. Change, 8(5): 421–428, https://doi.org/10.1038/s41558-018-0138-5, 2018.

Sheffield, J., Wood, E. F., Roderick, M. L.: Little change in global drought over the past 60 years. Nat. 491(7424), 435–438, https://doi.org/10.1038/nature11575, 2012.

Sorokin, Y., Jane Zelikova, T., Blumenthal, D., Williams, D. G., Pendall, E.: Seasonally contrasting responses of evapotranspiration to warming and elevated CO_2 in a semi-arid grassland. Ecohydrol. e1880, https://doi.org/10.1002/eco.1880, 2017.

Sophocleous, M.: Interactions between ground water and surface water: the state of the science. Hydrogeol. J. 10(2), 348–348, https://doi.org/10.1007/s10040-001-0170-8, 2002.

Swann, A. L., Hoffman, F. M., Koven, C. D., Randerson, J. T.: Plant responses to increasing CO_2 reduce estimates of climate impacts on drought severity. Proc. Natl. Acad. Sci. USA 113, 10019–10024, https://doi.org/10.1073/pnas.1604581113, 2016.

Thiery, W., Davin, E. L., Lawrence, D. M., et al.: Present-day irrigation mitigates heat extremes. J. Geophys. Res.: Atmos. 122, 1403–1422, https://doi.org/10.1002/2016JD025740, 2017.

Trenberth, K. E., Dai, A., Van Der Schrier, G., Jones, P. D., Barichivich, J., Briffa, K. R., Sheffifield, J.: Global warming and changes in drought. Nat. Clim. Change 4(1), 17–22, https://doi.org/10.1038/NCLIMATE2067, 2014.

Teuling, A. J., De Badts, E. A. G., Jansen, F. A., Fuchs, R., Buitink, J., Hoek Van Dijke, A. J., Sterling, S. M.: Climate change, reforestation/afforestation, and urbanization impacts on evapotranspiration and streamflow in Europe. Hydrol. Earth Syst. Sci., 23(9), 3631-3652, https://doi.org/10.5194/hess-23-3631-2019, 2019.

Van der Schrier, G., Jones, P. D., Briffa, K. R.: The sensitivity of the PDSI to the Thornthwaite and Penman-Monteith parameterizations for potential evapotranspiration. J. Geophys. Res.: Atmos. 116, D03106, https://doi.org/10.1029/2010JD015001, 2011.

van der Sleen, P., Groenendijk, P., Vlam, M., et al.: No growth stimulation of tropical trees by 150 years of CO_2 fertilization but water-use efficiency increased. Nat. Geoscience 8(1), 24–28, https://doi.org/10.1038/NGEO2313, 2015.

Wagle, P., Xiao, X., Scott, R. L., Kolb, T. E., Cook, D. R., Brunsell, N., Baldocchi, D. D., Basara, J., Matamala, R., Zhou, Y., and Bajgain, R.: Biophysical controls on carbon and water vapor fluxes across a grassland climatic gradient in the United States, Agr. Forest Meteorol., 214/215, 293–305, https://doi.org/10.1016/j.agrformet.2015.08.265, 2015.

Williams, C. A., Reichstein, M., Buchmann, N., Baldocchi, D., Beer, C., Schwalm, C., Wohlfahrt, G., Hasler, N., Bernhofer, C., Foken, T., Papale, D., Schymanski, S., and Schaefer, K.: Climate and vegetation controls on the surface water balance: Synthesis of evapotranspiration measured across a global network of flux towers, Water Resour. Res., 48, W06523, https://doi.org/10.1029/2011WR011586, 2012.

Williams, I. N. and Torn, M. S.: Vegetation controls on surface heat flux partitioning, and land-atmosphere coupling, Geophys. Res. Lett., 42, 9416–9424, https://doi.org/10.1002/2015gl066305, 2015.

Wei, Z., Yoshimura, K., Wang, L., Miralles, D. G., Jasechko, S., Lee, X. H.: Revisiting the contribution of transpiration to global terrestrial evapotranspiration, Geophys. Res. Lett., 44, 2792–2801, https://doi.org/10.1002/2016GL072235, 2017.

Yang, Y. T., Roderick, M. L., Zhang, S., McVicar, T. R., Donohue, R. J.: Hydrologic implications of vegetation response to elevated CO_2 in climate projections. Nat. Clim. Change 9: 44–48. https://doi.org/10.1038/s41558-018-0361-0, 2019.

Yang, Y. T., Zhang, S. L., Roderick, M. L., McVicar, T. R., Yang, D. W., Liu W. B., Li X. Y.: Comparing Palmer Drought Severity Index drought assessments using the traditional offline approach with direct climate model outputs. Hydrol. Earth Syst. Sci. 24: 2921–2930. https://doi.org/10.5194/hess-24-2921-2020, 2020.

Yin, J. B., Gentine, P., Zhou, S., Sullivan, S. C., Wang, R., Zhang, Y., Guo S. L.: Large increase in global storm runoff extremes driven by climate and anthropogenic changes. Nat. Commun. 22, 9(1): 4389, https://doi.org/10.1038/s41467-018-06765-2, 2018.

Yin, L., Fu, R., Shevliakova, E., Dickinson, R. E.: How well can CMIP5 simulate precipitation and its controlling processes over tropical south America?. Clim. Dynam. 41(11-12), 3127–3143, https://doi.org/10.1007/s00382-012-1582-y, 2013.

Zeng, Z., Ziegler, A. D., Searchinger, T., et al.: A reversal in global terrestrial stilling and its implications for wind energy production. Nat. Clim. Change 9, 1–7, https://doi.org/10.1038/s41558-019-0622-6, 2019.

Zhao, W.L., Gentine, P., Reichstein, M., Cook, B.I., Zhang, Y., Hagemann, S., Lorenz, R., Seneviratne, S. I., Gentine, P.: Physics-constrained machine learning of evapotranspiration. Geophys. Res. Lett. 46(24): 14496–14507, https://doi.org/10.1029/2019GL085291, 2019.

Zhou, C., Wang, K.: Biological and environmental controls on evaporative fractions at AmeriFlux sites. J. Appl. Meteorol. Clim. 55, 145–161. https://doi.org/10.1175/JAMC-D-15-0126.1, 2016.

Zhou, S., Williams, A. P., Berg, A. M., et al.: Land–atmosphere feedbacks exacerbate concurrent soil drought and atmospheric aridity. Proc. Natl. Acad. Sci. USA 116(38): 18848–18853, https://doi.org/10.1073/pnas.1904955116, 2019.